https://doi.org/10.48048/tis.2023.6396

An Environmental Approach in Production of Activated Carbon Monolithic Derived from Garlic Peels for Supercapacitor Application

Erman Taer[1,*], Apriwandi Apriwandi[1], Widya Sinta Mustika[1,2], Miftah Ainul Mardiah[1] and Rika Taslim[3]

[1]*Department of Physics, Riau University, Riau 28293, Indonesia*
[2]*Departement of Maintenance and Repair Engineering, Polytechnic of Kampar, Riau 28461, Indonesia*
[3]*Departement of Industrial Engineering, Islamic State University of Sultan Syarif Kasim, Riau 28293, Indonesia*

([*]Corresponding author's e-mail: erman.taer@lecturer.unri.ac.id)

Received: 13 September 2021, Revised: 25 October 2021, Accepted: 1 November 2021, Published: 24 November 2022

Abstract

An environmental approach is needed in the production of activated carbon as electrode material in supercapacitor applications. Activated carbon provides high specific surface area and well-developed pore structures. These circumstances compromise high electrochemical performance for supercapacitor. Therefore, this research focusses on fabricating the activated carbon derived from garlic peels through the chemical activation of potassium hydroxide under various concentrations, combined with 1-integrated stage pyrolysis. The morphology of activated carbon was observed using scanning electron microscopy (SEM), embedded in energy dispersive X-ray (EDS) for analyzing the elemental status. The crystalline degree of the activated carbon was observed using X-ray diffraction (XRD). The electrochemical performances of cell supercapacitor-based-ACM electrodes were evaluated with cyclic voltammetry (CV) and galvanostatic charging-discharging (GDC). The activated carbon was prepared in monolithic form without binder materials and shows a sponge liked-porous structure with high electrochemical performance, including specific capacitance of 204 F g^{-1}, with energy and power of 28.58, 71.16 W kg^{-1} under current densities 1 A g^{-1}, in the 2-electrode system of 1 M H_2SO_4 electrolyte. The results showed that using an environmental approach in the production of activated carbon monolithic derived from garlic peels has high electrochemical performance.

Keywords: Activated carbon, Monolithic, Garlic peels, Electrode, Supercapacitor

Introduction

A supercapacitor is a well-known alternative green technology with zero carbon waste to store energy and recover fossil exploitation [1,2]. Its advantages are long cycle life, fast charge-discharge, and excellent energy performance [3]. The supercapacitor's energy performance ranges between batteries and conventional capacitors. However, its power density is lower than conventional capacitors (P, > 10 kW kg^{-1}), with its energy density performed under batteries (E, > 7 Wh kg^{-1}) [4]. Therefore, numerous studies have been carried out on ways to enhance the level of energy density in supercapacitors to narrow the gap in batteries.

A well-designed of electrode materials have been concerned to put on high-level electrochemical performance. This is in addition to the development and classification of some electrode materials in activated carbon [5,6], conducting polymer [7,8], and transition metal oxide materials [9,10]. Studies on electrode material have been attractively conducted on the activated carbon, compromising high specific surface area and well-developed pore structures [11,12]. Biomass is the most common material used as a precursor for constructing activated carbon electrodes because it is priceless, easily processed, and environmentally friendly [13,14]. Biomass based-plants have been widely explored in the production of activated carbon material, such as fruit [15], flower [16], leaves [17], stem [18,19], bunch [20], and grass [21]. Presently, studies have been carried out on the use of plant seed as activated carbon materials [22], including fresh seed [23] and seed wasted-peels [24].

Furthermore, a great potential of garlic peels has been recommended for activated carbon electrodes, in which a high initial carbon yield of 46.48 % [25]. Zhang *et al*. (2018) stated that 3D pores structure of activated carbon derived garlic peels by chemically activated in the high level up a ratio of potassium hydroxide (KOH) [26]. Meanwhile, Teng (2020) also researched activated carbon from garlic

peels using KOH activation and irradiation of ultrasonic waves to improve the specific surface area [27]. However, these studies only focused on fabricating activated carbon in powder form, which is dusting with low mechanical strength.

In powder form, it is usually mixed with binder materials in assembly on supercapacitor cells, which blocked the ion penetration path [28]. This tends to level down the electrical conductivity as well as lowering the energy density [29]. Furthermore, the binder materials used is concerned with ineffective cost in production [30]. Additionally, both binder material and the high-level ratio of activated agent used remains environmental impact. Therefore, alternative treatment in low chemical materials is needed to ensure eco-environmental activated carbon electrode-based biomass production.

Some biomasses were treated as a monolithic form of activated carbon to ensure a low chemically activated process and avoid binder materials. The monolithic maintain for high electrical conductivity and ion adsorption, obviously producing high specific capacitance [14]. Also, the monolithic form shows a higher energy density comparative to powder form. For example, a rubber wood waste activated in low H_3PO_4 (10 % w/v) exhibited a high capacitance of 129 F g^{-1} under an energy density of 14.2 Wh kg^{-1} [3]. Eucalyptus and olive stone prepared in monolithic form showed a specific capacitance of 161 F g^{-1} and 217 F g^{-1}, respectively [31]. Recently, banana leaves performed in low chemically activated KOH exhibited excellent energy performance, including specific capacitance (C, 245 F g^{-1}) and energy density (P, 36.67 Wh kg^{-1}) [32].

In this research, garlic peels carbon was chemically activated in the low-level ratio of KOH (≤0.75 M) to obtain self-adhesive properties, which is used on monolithic coin liked-shape electrodes without binder materials. Subsequently, the monolithic electrode was converted into activated carbon through the 1-integrated pyrolysis stage of both carbonization (N_2/600 °C) and physical activation (CO_2/850 °C) and was represented through the density changes of the electrode. Physical characterization was evaluated using scanning electron microscopy (SEM), Energy Dispersive X-ray (EDX), X-ray diffraction (XRD). Also, electrochemical properties of the electrode were performed using cyclic voltammetry (CV) and Galvanic Charge-Discharge (GCD) in a 2-electrode system.

Materials and methods

Materials and instruments

Garlic peels (local product) were obtained from Traditional marketplace of Panam, Riau Province, Indonesia, potassium hydroxide (KOH) and sulfate acid (H_2SO_4) were in Merck KGa, Germany, DI water was purchased from Chemical Laboratory of University of Riau, Indonesia, pH-indicator strips (MColorpHast™). Tubular Furnace was designed by Payun Tech company from Indonesia, scanning electron microscopy (SEM) and energy dispersive X-ray (EDS) were in JEOL-JSM-6510-LA from Japan, X-ray diffraction (XRD) was Philip X-Pert Pro-PW3060/10, from Netherlands, cyclic voltammetry (CV, CV-UR Rad-Er 5841) and galvanostatic charging-discharging (GDC, CD-UR-Rad-Er 2018) were self-designed by University of Riau, Indonesia, that have been calibrated with standard instrument in error of ± 6 %.

Preparation of ACM electrodes

The activated carbon monolithic (ACM) electrodes were obtained using natural garlic peels (Traditional marketplace of Panam, Riau Province, Indonesia), oven-dried, and successively pre-carbonized to the temperature of 250 °C for 2.5 h. The obtained intermediate product was powdered through a set of mill instrument and sieved for homogeneous powder with its size less than 53 μm. Subsequently, the powdered product was chemically activated using a solution of potassium hydroxide (KOH) (Merck KGa, Germany), prepared in various concentrations of 0.25, 0.50 and 0.75 m. The activated powder products were pelletized into monolithic coin-liked shape form through a set of hydraulic press instrument operated on 8 ton mass loaded. Furthermore, each monolithic sample was converted into an ACM product through 1-stage integrated pyrolysis, using the carbonization (N_2/600 °C) and physical activation (CO_2/850 °C) processes. After the sample has cooled down, the products of activated carbon were immersed into DI water to measure the pH level (pH-indicator strips, MColorpHast™). The DI water was refilled and its pH was checked every 24 h until the pH level of 7. Finally, the products were labeled for ACM-x, where x denotes KOH concentration.

Physical characterization

The ACM samples were characterized in the dimensional density with the morphologies evaluated using scanning electron microscopy (SEM, JEOL-JSM-6510-LA, Japan), embedded in energy dispersive X-ray (EDS) for analyzing the elemental status on the surface of a sample, operated at 15 kV. The crystalline degree of the samples was observed using X-ray diffraction (XRD, Philip X-Pert Pro-PW3060/10, Netherlands), applied in Cu-Kα radiation (Kα=1.5418 Å). The interlayer spacing (d_{002} and d_{100}) and microcrystalline dimension (L_c and L_a) were calculated based on Bragg's Law and Debye-Scherer Equation, respectively.

Electrochemical measurement

The ACM samples were first immersed in an aqueous electrolyte in 1 m H_2SO_4 (Merck KGa, Germany). Priors to electrochemical analysis, the electrodes of ACM were polished in the thickness level of 0.2 mm, assembled in sandwich-like layers, in accordance with preliminary studies [33,34]. Two ACM electrodes were prepared on the current collector plate (d = 0.4 mm, stainless steel), separated by a separator membrane (duck eggshell). Subsequently, the assembled electrodes were covered using a acrylic body cell and a teflon rod circled. The electrochemical performances of cell supercapacitor-based-ACM electrodes were evaluated in the 2-electrode cell with cyclic voltammetry (CV, CV-UR Rad-Er 5841, University of Riau, Indonesia) and galvanostatic charging-discharging (GDC, CD-UR-Rad-Er 2018, University of Riau, Indonesia). CV and GDC were scan rates of 1 mV s^{-1} and 1 A g^{-1}, respectively, operating in the potential of 1 V. The specific capacitance (C, F g^{-1}), specific energy (E, Wh kg^{-1}), and specific power (P, W kg^{-1}) were calculated in the standard equation.

Results and discussion

Monolithic characteristic

The monolithic characteristic was performed in density parameter, which shrank after the pyrolysis treatment of ACM, as shown in **Figure 1**. The density shrinkage was evaluated on the mass losses, diameter, and decline in thickness with the release of activated carbon's mass by non-carbon materials determined in 2 stages. First, some elemental volatiles such as oxygen, hydrogen, and nitrogen were released at high temperatures by the carbonization treatment. Second, carbon monoxide was produced as residual products of physical activation by CO_2 [35,36]. Additionally, KOH impregnated bubbled during pyrolysis and increased the volatiles removal. These mass losses were carried out to produce some vacancies on the carbon atom, thereby leading to the rearrangements of its chains. This circumstance tends to decrease the ACM dimension, namely diameter, and thickness. However, the highest concentration of KOH of 0.75 m led to high density, with less bubbles and some solid K-byproducts.

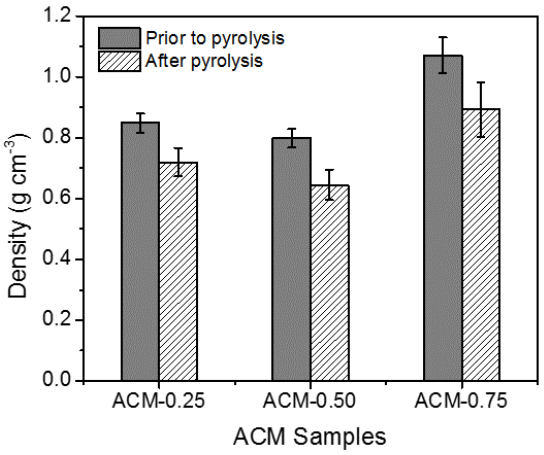

Figure 1 Density diagram of ACM.

The ACM samples density was found in the range of 0.64 - 0.89 g cm^{-3}, which is fit for activated carbon-based biomass materials for the monolithic formed. For example, the density values in the ranges of 0.64 - 1.02 g cm^{-3} were reported for the activated carbon monolithic from *Areca catechu* husk, which

was chemically activated by KOH [33]. Activated carbon monolithic based green stem of cassava demonstrated the density between 0.61 - 0.93 g cm^{-3} [34]. Furthermore, the low density ($\rho \leq 0.75$ g cm^{-3}) is predicted in sponge-liked porosity and is expected for better ion penetration and high electrochemical performance [37].

Morphology analysis

The morphology structure of ACM was evaluated using scanning electron microscopy (SEM), as shown in **Figure 2**. The nanofiber structures were observed on the aggregate surface, sizing of 80 - 102 nm (**Figures 2(a) - 2(c)**), and were extracted on cellulose compound inside raw garlic peels through an alkaline reaction of KOH [38]. In addition, the nanofiber structures were also obtained in activated carbon-based biomass material and the macropore between the aggregates were revealed [33,34]. This result is associated with the chemical activation of KOH on the active sites of carbon material [39]. Accordingly to the magnified SEM analysis (**Figures 2(d) - 2(e)**), many pores exist on the walls of aggregate. This is attributed to the potassium vapor, which is diffused into the deep carbon layer as physical activation treatment (CO_2/850 °C) and eventually generating new pores [40].

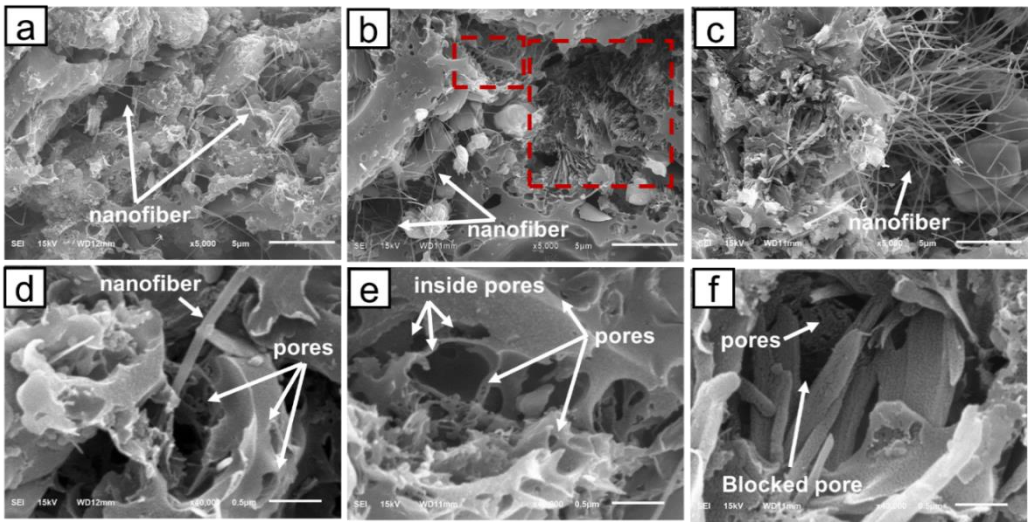

Figure 2 SEM image, (a) ACM - 0.25, (b) ACM - 0.50, (c) ACM - 0.75, d) enlarged (a), (e) enlarged (b), (f) enlarged (c).

The sponge-liked porous structure was depicted by ACM - 0.50 and remarked in **Figures 2(b) - 2(e)** shows that some pore existed on the inside layer of the aggregate due to the presence of an increased concentration of KOH. Furthermore, this sponge-liked porous contributes to the accessible surface for ion pairs formation and enhances electrochemical performance [26]. The fiber density for ACM - 0.75 increased with a decline in pores structures in which impregnated KOH produce less bubbling and more crystalizing by K-byproducts, as confirmed on the EDS analysis in the next subsection. This crystallized product generated the blocked pores (**Figure 2(f)**) and increased the internal resistance of materials.

Microstructure analysis

The microstructure characteristics were analyzed on an XRD diffractogram, as shown in **Figure 3**. It consists of 2 broadening peaks in the range of 24.152 - 25.673 ° and 44.657 - 46.515 °, reflecting a carbon plane of 002 and 100, respectively (JCPDS No. 41 - 1487). These degrees correspond to the amorphous structure, typically for porous carbon-based biomass [41]. The porous structure contributes to etch carbon-compound chains by activation process and rearranging carbon atoms [14]. Some sharp peaks were found, which indicated the presence of impurities at the peak of 29 ° (JCPDS No. 89 - 1668) for SiO_2, while 37 ° and 39° were obtained for $CaCO_3$ (JCPDS.82 - 1690). These materials were also found as a residual product of the pyrolysis process on biomass [34].

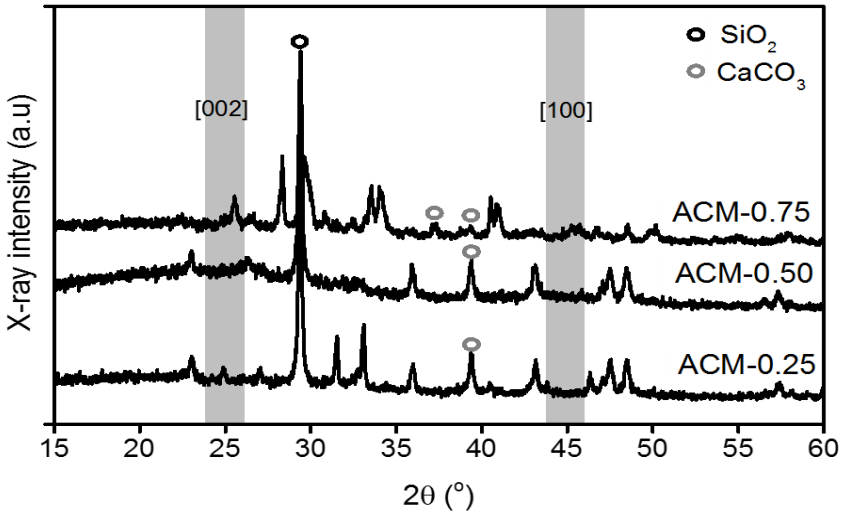

Figure 3 X-ray diffractogram of ACM samples.

The value of the microstructure parameter is shown in **Table 1**. According to Bragg Law, the interlayer space (d_{002} and d_{100}) is in the range of 3.670 - 3.682 and 1.951 - 2.028, which is ideal for amorphous structure on porous carbon material [20]. However, the d_{002} of ACM - 0.75 is 3.467, which slightly tends to graphite structure [41]. It is associated with high impurity in crystalline degree, thereby affecting the reflecting plane of carbon. This impurity is confirmed in the EDS analysis on next subsection. The microcrystalline structures (L_c and L_a) were calculated using the Debye-Scherer equation. The ACM - 0.50 shows that the L_c and L_a are potential for high microporosity. This is supported by an SEM image on sponge-like porous, which is explained in the above subsection. Based on the empirical formula from Kumar, the low L_c provide a large surface active area, thereby enhancing a cumulative of ion pairs formation, which given in Eqs. (1) - (2) [42].

$$SSA_{XRD} = \frac{2}{\rho_{XRD} L_c} \quad (1)$$

$$\rho_{XRD} = \left(\frac{d_{002\,(graphite)}}{d_{002}}\right) \rho_{graphite} \quad (2)$$

Where SSA_{XRD} is specific surface area ($m^2\ g^{-1}$), $d_{002(graphite)}$ determines as interlayer spacing of graphite ($d_{002(graphite)}$ = 3.3354 Å). Also, $\rho_{graphite}$ is density of graphite ($\rho_{graphite}$ = 2.268 g cm^{-3}). ρ_{XRD} denotes density of activated carbon in graphite structure. These data assumed, the higher SSA_{XRD} provide more ion pairs formation.

Table 1 The interlayer space (d_{002} and d_{100}) and microcrystalline structure (L_c and L_a).

Samples	$2\theta_{002}$ (°)	$2\theta_{100}$ (°)	d_{002} (Å)	d_{100} (Å)	L_c (Å)	L_a (Å)	SSA_{XRD} ($m^2\ g^{-1}$)
ACM - 0.25	24.233	45.612	3.670	1.987	13.003	7.423	746.211
ACM - 0.50	24.152	46.515	3.682	1.951	12.372	4.511	786.832
ACM - 0.75	25.673	44.657	3.467	2.028	16.144	16.728	567.782

Elemental status

The elemental status of ACM samples was analyzed using the EDS technique, as shown in **Table 2**. The increase in concentration of KOH, led to a rise in carbon (C) contents for ACM - 0.25 and ACM - 0.50 from 74.19 - 78.09 %, with a decrease in oxygen (O) contents. Also, each sample gradually decreased in the composition of calcium (Ca), magnesium (Mg), and silicon (Si) due to the degradation of carbon compounds during the pyrolysis process. Mineral contents were also found out as elemental basic

in biomass materials [43]. In addition, the KOH impregnation generated C-compounds etching, thereby increasing C contents and contributing to high electrochemical performance [33]. Meanwhile, potassium (K) contents surprisingly increased the level by 10.56 %. This process was obtained due to the incomplete removal of the K-byproduct. However, the excessive concentration of KOH, the C contents for ACM - 0.75 dramatically decreased due to the high level of K-byproducts, leading to low C-compounds etching. This was also found in the heteroatom compositions, which are sodium (Na), sulfur (S), and chlorine (Cl).

Table 2 Elemental contents.

Samples	Elemental contents								
	C (%)	O (%)	Ca (%)	Mg (%)	Si (%)	K (%)	Cl(%)	Na (%)	S (%)
ACM - 0.25	74.19	21.54	3.26	0.36	0.66	0.00	0.00	0.00	0.00
ACM - 0.50	78.09	16.35	0.24	0.35	0.38	4.59	0.00	0.00	0.00
ACM - 0.75	55.76	27.39	1.72	0.20	0.31	10.56	3.05	0.58	0.44

Electrochemical performance

Set electrochemical tests were performed to evaluate the electrochemical behavior of the activated carbon monolithic derived from garlic peels. The CV and GDC results for activated carbon electrode-based garlic peels in 1 M H_2SO_4 electrolyte are shown in **Figure 4**. Each sample depicts a rectangular-liked shape of CV curve, corresponding to electrochemical double-layer capacitance (EDLC), which was also found in every electrode material based-activated carbon biomass, prepared without binder material [26,32]. Based on the current and CV areas, ACM - 0.50 has the highest specific capacitance of 192 F g^{-1}, which is 42 and 400 % higher than ACM - 0.25 and ACM - 0.75, respectively. The high capacitance is related to the sponge-liked porous structure, serving a large accessible surface area for ion pairs formation.

Figure 4(b) shows different CV curves for ACM - 0.50 at various scan rates, with each generating a rectangular-liked shape in a double-layer mechanism. However, a straight line in the CV curve as the initial charging process had a scan rate of 1 mV s^{-1}, thereby indicating a spontaneous charging mechanism. Although, the ramping step was observed on the CV curve as a scan rate of 2 mV s^{-1}, indicating a series resistance for the charging process. For other samples within a higher scan rate above 2 mV s^{-1}, the CV curves are non-ideal double-layer capacitance due to low ion transfer inside pores of sponge-liked porous.

The specific capacitance at various scan rates for the ACM sample is shown in **Figure 4(c)**. The specific capacitance is dramatically decreased at a scan rate of 1 - 2 mV s^{-1}, which is dropped into 55 and 44 % for ACM - 0.25 and ACM - 0.50, respectively. Meanwhile, as the scan rate increased above 2 mV s^{-1}, each sample gradually decreased the specific capacitance. At a scan rate of 10 mV s^{-1}, these specific capacitances remained at the level of 35, 28 and 35 %, respectively, for ACM - 0.25, ACM - 0.50 and ACM - 0.75. This is associated with a narrow path used to get insides pore in ion penetration, which is slow in the charge-discharge mechanism.

Figure 4(d) illustrates the GDC curves of ACM samples at a current density of 1 A g^{-1}, which showed a nonlinear triangular liked shape. These curves correspond to the EDLC mechanism, containing low faradaic reaction by imperfectly elemental heteroatom [30,32]. It also shows an asymmetrical triangular curve, compromising charged processes that are longer than the discharge and linked to the appearance of series resistance from the narrow path in ion penetration. According to GDC curves, the highest specific capacitance is 204 F g^{-1} (ACM - 0.50), followed by ACM - 0.25 (162 F g^{-1}) and ACM - 0.75 (37 F g^{-1}). This is caused the sponge liked-porous providing better pores structure for large cumulative of ion pairs formation. Also, it correlated to the internal resistance of ACM, corresponding to 0.020 Ω (ACM - 0.25), 0.008 Ω (ACM - 0.50) and 0.075 Ω (ACM - 0.75).

The energy and power densities were calculated in the standard equation of 28.58 and 71.16 W kg^{-1}, respectively. These values are low compared to the previously reported ones used in activated carbon electrodes derived from garlic peels, the monolithic form of activated carbon applied as an electrode in a supercapacitor exhibits high energy density [26]. The monolithic form was adjusted to combine the sponge liked-porous and easy-accessible carbon surface. The sponge porous structure was developed on chemically activation using KOH. The inside pore of the sponge structure tends to size in micropore ranges, producing abundant cumulative ion pairs [44]. Furthermore, the micropores tend to generate a

narrow path for ion transfer and decrease the rate of charge-discharge [24]. Meanwhile, a binder-free method in monolithic electrode attained the electrical conductivity on the active sites of carbon surface, thereby enhancing the interaction between carbon surface and electrolyte ions.

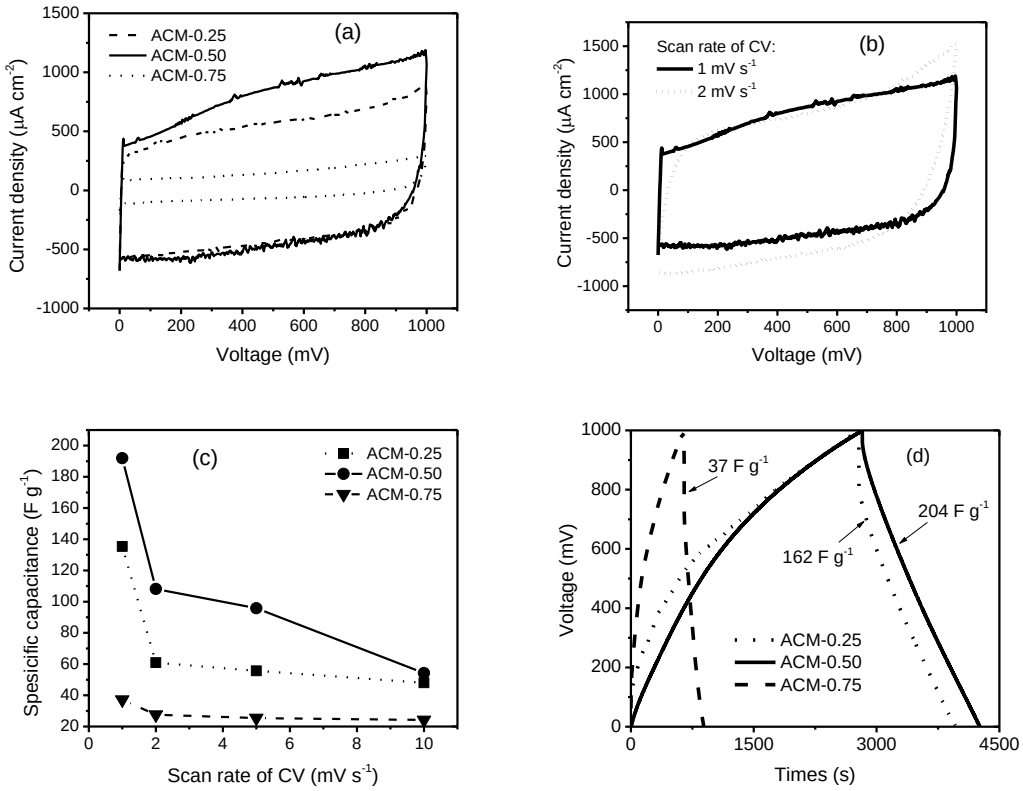

Figure 4 (a) CV curves of ACM samples at a scan rate of 1 mV s^{-1}, b) CV curves of ACM - 0.50 at various scan rate, (c) specific capacitances at various scan rate for ACM samples, (d) GDC profile of ACM electrode at a scan rate of 1 mV s^{-1}.

Conclusions

The activated carbon monolithic derived from garlic peels were successfully synthesized using a low chemically activated route. The fabrication was determined in various concentrations of potassium hydroxide as an activating agent, such as 0.25, 0.50 and 0.75 M. The activated carbon was synthesized via 1-integrated stage pyrolysis both carbonization (N_2/600 °C) and physical activation (CO_2/850 °C). The monolithic density was evaluated, and the relationship between the physical characteristic and electrochemical performance were analyzed. The result showed the amorphous structure with high carbon yields (78.09 %) under optimal conditions. Most interestingly, a unique structure of sponge-liked porous was enabled and put on high electrochemical performance, including a specific capacitance of 204 F g^{-1}. Furthermore, it performs energy and power density of 28.58 and 71.16 W kg^{-1}, respectively, at current densities of 1 A g^{-1}. This electrode was performed in 2-electrode systems consisting of 1 M H_2SO_4 electrolyte, without binder materials. The results highlight an environmental route for fabricating electrode materials from biomass for high electrochemical performance.

References

[1] BK Sovacool and S Griffiths. The cultural barriers to a low-carbon future: A review of six mobility and energy transitions across 28 countries. *Renew. Sustain. Energ. Rev.* 2019; **119**, 109569.

[2] B Zakeri and S Syri. Electrical energy storage systems: A comparative life cycle cost analysis. *Renew. Sustain. Energ. Rev.* 2015; **42**, 569-96.

[3] D Lefebvre and FH Tezel. A review of energy storage technologies with a focus on adsorption thermal energy storage processes for heating applications. *Renew. Sustain. Energ. Rev.* 2017; **67**, 116-25.

[4] S Koohi-Fayegh and MA Rosen. A review of energy storage types, applications and recent developments. *J. Energ. Storage* 2020; **27**, 101047.

[5] O Fasakin, JK Dangbegnon, DY Momodu, MJ Madito, KO Oyedotun, MA Eleruja and N Manyala. Synthesis and characterization of porous carbon derived from activated banana peels with hierarchical porosity for improved electrochemical performance. *Electrochim. Acta* 2018; **262**, 187-96.

[6] A Durairaj, T Sakthivel, S Ramanathan, A Obadiah and S Vasanthkumar. Conversion of laboratory paper waste into useful activated carbon: A potential supercapacitor material and a good adsorbent for organic pollutant and heavy metals. *Cellulose* 2019; **26**, 3313-24.

[7] L Yang, J Henzie, T Park, J Wang, C Young, H Xie, JW Yi, J Li, M Kim, J Kim, Y Yamauchi and J Na. Fabrication of flexible microsupercapacitors with binder-free zif-8 derived carbon films via electrophoretic deposition. *Bull. Chem. Soc. Jpn.* 2020; **93**, 176-81.

[8] C Wang, J Kim, J Tang, J Kim, H Lim, V Malgras, Y You, Q Xu, J Li and Y Yamauchi. New strategies for novel mof-derived carbon materials based on nanoarchitectures. *Chemistry* 2020; **6**, 1-22.

[9] NLW Septiani, YF Kaneti, KB Fathoni, J Wang, Y Ide, B Yuliarto, Nugraha, HK Dipojono, A Nanjundan, D Golberg, Y Bando and YN Yamauchi. Self-assembly of nickel phosphate-based nanotubes into two-dimensional crumpled sheet-like architectures for high-performance asymmetric supercapacitors. *Nano Energ.* 2019; **67**. 104270.

[10] S Makino, Y Yamauchi and W Sugimoto. Synthesis of electro-deposited ordered mesoporous RuO x using lyotropic liquid crystal and application toward micro-supercapacitors. *J. Power Sourc.* 2013; **227**, 153-60.

[11] H Ji, X Zhao, Z Qiao, J Jung, Y Zhu, Y Lu, LL Zhang, AH Macdonald and RS Ruoff. Capacitance of carbon-based electrical double-layer capacitors. *Nat. Comm.* 2014; **5**, 1-7.

[12] M Gopiraman, D Deng, B Kim, I Chung and IS Kim. Three-dimensional cheese-like carbon nanoarchitecture with tremendous surface area and pore construction derived from corn as superior electrode materials for supercapacitors. *Appl. Surf. Sci.* 2017; **409**, 52-9.

[13] AM Abioye and FN Abi. Recent development in the production of activated carbon electrodes from agricultural waste biomass for supercapacitors: A review. *Renew. Sustain. Energ. Rev.* 2015; **52**, 1282-93.

[14] Y Wang, Q Qu, S Gao, G Tang, K Liu, S He and C Huang. Biomass derived carbon as binder-free electrode materials for supercapacitors. *Carbon* 2019; **155**, 706-26.

[15] S Ahmed, M Rafat and A Ahmed. Nitrogen doped activated carbon derived from orange peel for supercapacitor application. *Adv. Nat. Sci.* 2018; **9**, 035008.

[16] F Wu, J Gao, X Zhai, M Xie, Y Sun, H Kang and Q Tian. Hierarchical porous carbon microrods derived from albizia flowers for high performance supercapacitors. *Carbon* 2019; **147**, 242-51.

[17] Q Lu, S Zhou, B Li, H Wei, D Zhang, J Hu, L Zhang, J Zhang and Q Liu. Mesopore-rich carbon flakes derived from lotus leaves and it's ultrahigh performance for supercapacitors. *Electrochim. Acta* 2020; **333**, 135481.

[18] G Zhang, Y Chen, Y Chen and H Guo. Activated biomass carbon made from bamboo as electrode material for supercapacitors. *Mater. Res. Bull.* 2018; **102**, 391-8.

[19] M Danish and T Ahmad. A review on utilization of wood biomass as a sustainable precursor for activated carbon production and application. *Renew. Sustain. Energ. Rev.* 2018; **87**, 1-21.

[20] R Farma, M Deraman, A Awitdrus, IA. Talib, E Taer and NH Basri. Preparation of highly porous binderless activated carbon electrodes from fibres of oil palm empty fruit bunches for application in supercapacitors. *Bioresource Tech.* 2013; **132**, 254-61.

[21] Q Tian, X Wang, X Xu, M Zhang, L Wang, X Zhao, Z An, H Yao and J Gao. A novel porous carbon material made from wild rice stem and its application in supercapacitors. *Mater. Chem. Phys.* 2018; **213**, 267-76.

[22] S Ahmed, A Ahmed and M Rafat. Supercapacitor performance of activated carbon derived from rotten carrot in aqueous, organic and ionic liquid based electrolytes. *J. Saudi Chem. Soc.* 2018; **22**, 993-1002.
[23] S Li, Q Chen, Y Gong, H Wang, D Li, Y Zhang, Q Fu and C Pan. One-step carbonization activation of garlic seeds for honeycomb-like hierarchical porous carbon and its high supercapacitor properties. *ACS Omega* 2020; **5**, 29913-21.
[24] S Kumagai and D Tashima. Electrochemical performance of activated carbons prepared from rice husk in different types of non-aqueous electrolytes. *Biomass Bioenergy* 2015; **83**, 216-23.
[25] T Ji, K Han, Z Teng, J Li, M Wang and J Zhang. Synthesis of activated carbon derived from garlic peel and its electrochemical properties. *Int. J. Electrochem. Sci.* 2021; **16**, 1-14.
[26] Q Zhang, K Han, S Li, M Li, J Li and K Ren. Synthesis of garlic skin-derived 3D hierarchical porous carbon for high-performance supercapacitors. *Nanoscale* 2019; **10**, 2427-37.
[27] Z Teng, K Han, J Li, Y Gao, M Li and T Ji. Ultrasonics - sonochemistry ultrasonic-assisted preparation and characterization of hierarchical porous carbon derived from garlic peel for high-performance supercapacitors. *Ultrason. Sonochem.* 2020; **60**, 104756.
[28] AE Ismanto, S Wang, FE Soetaredjo and S Ismadji. Preparation of capacitor's electrode from cassava peel waste. *Bioresource Tech.* 2010; **101**, 3534-40.
[29] K Fic, A Platek, J Piwek and E Frackowiak. Sustainable materials for electrochemical capacitors. *Mater. Today* 2018; **21**, 437-54.
[30] U Thubsuang, S Laebang, N Manmuanpom and S Wongkasemjit. Tuning pore characteristics of porous carbon monoliths prepared from rubber wood waste treated with H_3PO_4 or NaOH and their potential as supercapacitor electrode materials. *J. Mater. Sci.* 2017; **52**, 6837-55.
[31] PO Ibeh, FJ Garcia-Mateos, J Rosas, J Rodriguez-Mirasol and T Cordero. Activated carbon monoliths from lignocellulosic biomass waste for electrochemical applications. *J. Taiwan Inst. Chem. Eng.* 2019; **97**, 480-8.
[32] A Apriwandi, E Taer, R Farma, RN Setiadi and E Amiruddin. A facile approach of micro-mesopores structure binder-free coin/monolith solid design activated carbon for electrode supercapacitor. *J. Energ. Storage* 2021; **40**, 102823.
[33] E Taer, F Febriyanti, WS Mustika, R Taslim, A Agustino and A Apriwandi. Enhancing the performance of supercapacitor electrode from chemical activation of carbon nanofibers derived areca catechu husk via one-stage integrated pyrolysis. *Carbon Lett.* 2021; **31**, 601-12.
[34] E Taer, N Yanti, WS Mustika, A Apriwandi, R Taslim and A Agustino. Porous activated carbon monolith with nanosheet/nanofiber structure derived from the green stem of cassava for supercapacitor application. *Int. J. Energ. Res.* 2020; **44**, 10192-205.
[35] C Jiang, GA. Yakaboylu, T Yumak, JW Zondlo, M Edward and J Wang. Activated carbons prepared by indirect and direct CO_2 activation of lignocellulosic biomass for supercapacitor electrodes. *Renew. Energ.* 2020; **155**, 38-52.
[36] MA Yahya, Z Al-qodah and CWZ Ngah. Agricultural bio-waste materials as potential sustainable precursors used for activated carbon production: A review. *Renew. Sustain. Energ. Rev.* 2015; **46**, 218-35.
[37] C Romero-rangel, A Guillén-lópez, LM Mejía-mendoza, M Robles, ND Espinosa-torres and J Muñiz. Approaches on the understanding of nanoporous carbon reactivity with polyatomic ions. *Appl. Surf. Sci.* 2019; **495**, 143392.
[38] JL Espinoza-acosta, PI Torres-chávez, JL Olmedo-martínez, A Vega-rios, S Flores-gallardo and EA Zaragoza-contreras. Lignin in storage and renewable energy applications: A review. *J. Energ. Chem.* 2018; **27**, 1422-38.
[39] G Huang, Q Geng, B Xing, Y Liu and Y Li. Manganous nitrate -assisted potassium hydroxide activation of humic acid to prepare oxygen-rich hierarchical porous carbon as high-performance supercapacitor electrodes. *J. Power Sourc.* 2020; **449**, 227506.
[40] B Xu, Y Chen, G Wei, G Cao, H Zhang and Y Yang. Activated carbon with high capacitance prepared by NaOH activation for supercapacitors. *Mater. Chem. Phys.* 2010; **124**, 504-9.
[41] S Ghosh, R Santhosh, S Jenifer, V Raghavan, G Jacob, K Nanaji, P Kollu, SK Jeong and AN Grace. Natural biomass derived hard carbon and activated carbons as electrochemical supercapacitor electrodes. *Sci. Rep.* 2019; **9**, 16315.
[42] K Kumar, R Saxena, R Kothari, D Suri, K Kaushik and J Bohra. Correlation between adsorption and x-ray diffraction studies on viscose rayon based activated carbon cloth. *Carbon* 1997; **35**, 1842-4.

[43] J Pallarés, A González-cencerrado and I Arauzo. Production and characterization of activated carbon from barley straw by physical activation with carbon dioxide and steam. *Biomass Bioenergy* 2018; **115**, 64-73.

[44] X Song, X Ma, Y Li, L Ding and R Jiang. Tea waste derived microporous active carbon with enhanced double-layer supercapacitor behaviors. *Appl. Surf. Sci.* 2019; **487**, 189-97.